Strathprints Institutional Repository

( )
Low Impact Velocity Wastage in FBCs: Experimental Results and Comparison Between Abrasion and Erosion Theories

Chacon-Nava, J.G.[1], Almeraya-Calderon, F.[1] Martinez-Villafañe, A.[1] & Stack, M.M.[2]*
[1]Depto. Integridad y Diseño de Materiales Compuestos
Centro de Investigación en Materiales Avanzados, S.C.
Chihuahua, Chih., Mexico
**Corresponding Author*

[2]Department of Mechanical and Aerospace Engineering
University of Strathclyde
Glasgow, Scotland, U.K.

1. Introduction

The use of technologies related to combustion of coal in fluidized bed combustors (FBCs) present attractive advantages over conventional pulverized coal units. Some of the outstanding characteristics are: excellent heat transfer, low emission of contaminants, good combustion efficiencies and good fuel flexibility. However, FBC units can suffer materials deterioration due to particle interaction of solid particles with the heat transfer tubes immersed on the bed (Hou, 2004, Oka, 2004, Rademarkers et al., 1990). Among other issues, some of the most important factors believed to cause wear problems are: the motion of slowly but relatively coarse particles, particles loaded onto the surface by other particles, erosion by relatively fast-moving particles associated with bubbles, and abrasion by blocks of particles thrown into the surface by bubble collapse. Thus, erosion or abrasion processes can occur by a variety of causes. For the case of particle movement against in-bed surfaces, it has been suggested that there is no difference in the ability to cause degradation between solid particle erosion and low stress three body abrasion, and distinctions between the two forms of wear should not to be made (Levy, 1987).

1.1 The Most Commons Types of FBC´S

On applications such as steam and power generation, the most important types of FBCs are: 1) the atmospheric fluidized-bed combustor (AFBC). The superficial air velocity is between 1 and 3 m s^{-1}, to give a "bubbling bed"(Highley & Kaye, 1983); 2) The pressurized fluidized-bed combustor (PFBC). Here, the unit is operated at elevated pressure (from 6 up to 40 bar), and the main purpose is to expand the combustion products in a gas turbine to generate electricity through steam rising. Therefore, a higher efficiency of electricity generation is possible than that from either a gas or steam turbine plant alone (Howard, 1989); 3) the circulating fluidized-bed combustor (CFBC). In this system, the velocity of the fluidizing gas is significantly higher, being of a typical value about 5 m s^{-1} to 10 m s^{-1} than in the two previous systems. Fig. 1 shows a schematic diagram of the various FBC´S systems (Rademarkers & Ketunen, 1986).

1.2 Wastage Problems in FBC´S

Earlier studies on material behavior in FBCs suggested that wastage by particulate erosion did not represent a potential problem. A report considerer very unlikely that wastage would be a serious problem as the particle impact velocities are low, generally less than 5 m s^{-1}, (Mezko, 1977). Another study confirmed the above observations, since in their FB unit they did not found evidence of wastage on the in-bed tubes (Beacham & Marchall, 1979). However, despite the general good signs expressed above, since the early eighties, material wastage has been a recurrent problem in bubbling fluidized-bed combustors (AFBC and PFBC) throughout the world. For instance, wear rates of about 1 mm per 1000 h for in-bed tubes have been reported in a Chinese unit (Zhang, 1980). In the USA, observations of wastage of the in-bed tubes in several combustors have been reported (Kantesaria & Marchall, 1983, Montrone, 1983). In the UK, high wastage has been reported from the Grimethorpe plant, where wastages rates up to 1.7 mm per 1000 h were recorded on evaporator tubes (Anderson et al. 1987).

1.3 Wear Characteristics

It is not clear to what extent materials wastage can be attributed to mechanical phenomena such as erosion and/or abrasion by the fluidized bed particles (Stringer & Wright, 1987). Some of the most important factors believed to cause problems are: a) erosion by relatively slowly moving, but relatively coarse particles; b) wear by particles loaded onto the surface by other particles; c) erosion by relatively fast-moving particles associated with bubbles; d) intrinsic fast particles in the bed (apart from the fast particles in the

bubble wakes); e) erosion by fast moving particles immediately above the bed in the splash zone; f) erosion or abrasion associated with long range patterns; g) erosion induced by in-bed jets; h) abrasion by blocks of particles thrown into the surface by bubble collapse and i) wastage induced by the presence of geometrical irregularities

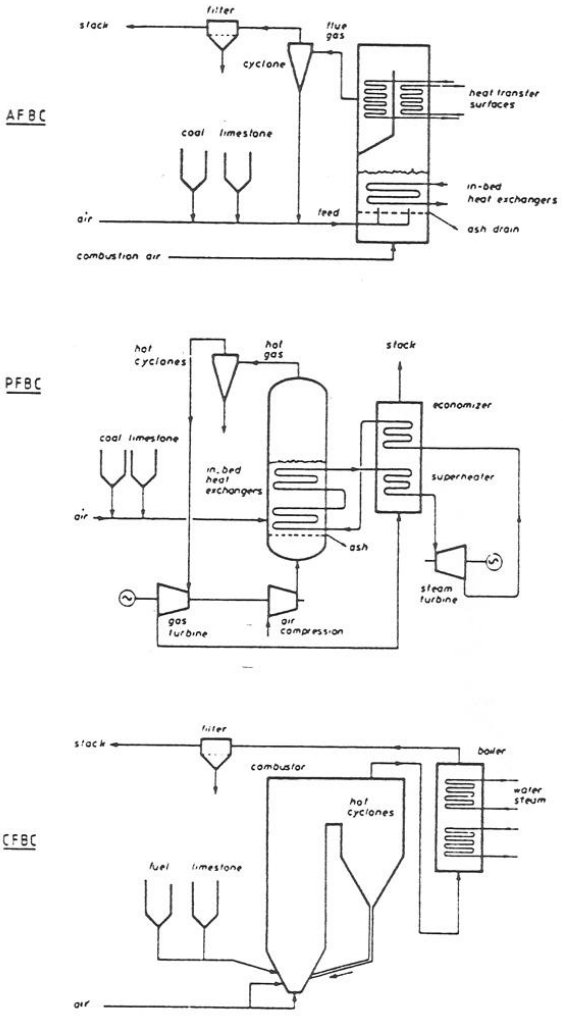

Fig. 1 Most common types of FBCs.

The wastage modes within a bed are not well understood because some of the above causes can be more closely related to a purely erosion process, for example c), e), f) and g), whereas others appears to be more related to a three-body abrasion process, for example b) and h). A general representation of the dense and bubble phase on an in-bed surface is presented in Fig. 2 (Janson, 1985)

Frames d) to f) are of interest regarding particle –tube interactions; in d) and e), changes in emulsion phase density can occur as conditions change in the fluidized bed, for example, fluidization behavior. In e), packing of the emulsion phase against an in-bed tube can be seen. Frame f) shows the case where a bubble. With a limited number of particles, is present at the bottom of a tube. For in-bed tubes, it is generally accepted that particle impact velocities range from 1 m s^{-1}, to 5 m s^{-1}. However, experimental determinations of particle velocities are difficult and rely on cold model studies. For instance, it has been reported that the average particle velocity was about 70% of the superficial velocity (Vs), but some particles had velocities as high as five times the values of Vs (Boiarski, 1978). Another study found that on bubble arrival at the tube surface, the particle velocity increases rapidly and streak across the tube surface, at velocities up to 5.6 m s^{-1}(Peeler & Whitehead, 1982). Another work found that particles do not move independently but as aggregates, and reported expressions giving the particle velocity, Vp, as function of the gas superficial velocity and impact angle, in the form (Tsutsumi et al., 1989):

$$Vp = 3.24\ Vs^{0.73} \quad \text{(at } 45^0 \text{ around the tube)} \qquad (1)$$

$$Vp = 1.99\ Vs^{0.89} \quad \text{(at normal impact angle)} \qquad (2)$$

As Vs is expressed in m s^{-1} the first expression (valid at shallow impact angles) predicts a particle impact velocity of 3.24 m s^{-1} at a superficial velocity of 1 m s^{-1}. However, since many FBC units typically operate at Vs about 2.5 m s^{-1}, particle velocities of about 6.2 m s^{-1} can be obtained.

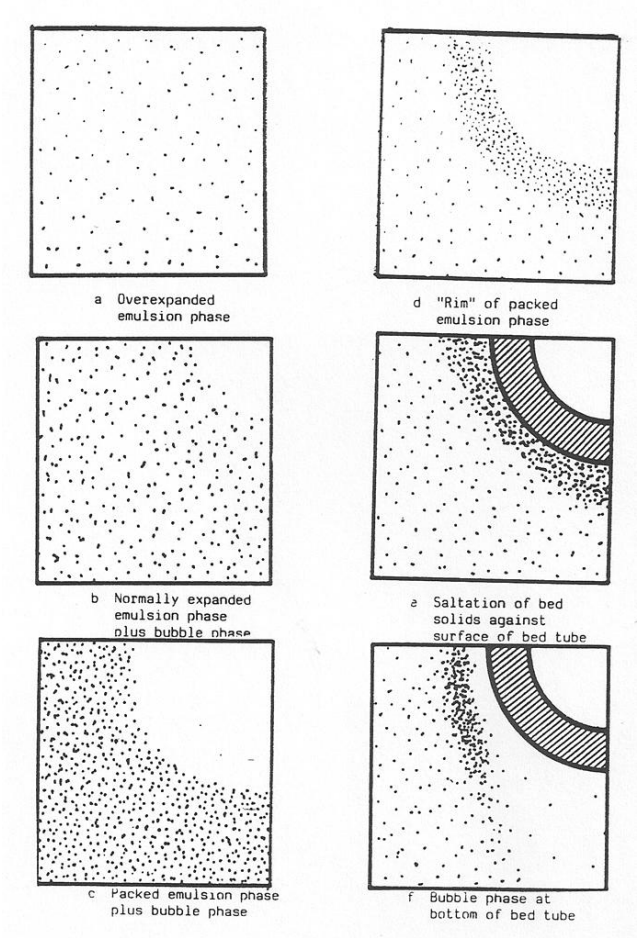

Fig. 2 A representation of variations in solid density in fluidized-bed bubble and emulsion phases.

1.4. Location of Maximum Wear

The maximum wear is normally located on in-bed tubes on the bottom half portion of the tubes, and appears in two patterns. In one, the wear is a maximum at positions about 20^0 – 30^0 on either side of the bottom, while wear is small or zero at the bottom. The second pattern has the maximum wear at the bottom of the tube, decreasing to zero typically at about 45^0. These patterns have been called "Class A" and "Class B" respectively (Stringer & Wright, 1987), and have been observed in cold simulations as well as in practical units (Anderson et al., 1987, Parkinson et al., 1985, Tsutsumi et al, 1989, Wang et al., 1992). It is interesting to note that Class A is related to the angle of impact corresponding to maximum wear in erosion of ductile metals. However, cold model studies speculates that, erosion is a maximum at normal impact angle, while abrasion is a maximum at about 35^0 on either side of the tube bottom (Wheeldon, 1990). Class B is more typical of the so-called brittle erosion. Fig. 3 shows both patterns which have been observed in real combustors.

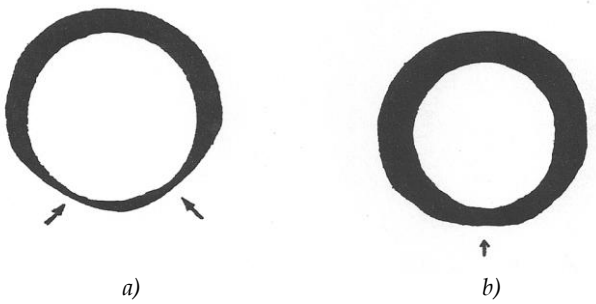

Fig. 3 Wastage patterns found in FBCs indicating with arrows the maximum location of wear: a) Class A, b) Class B.

As was mentioned before, erosion or abrasion (particularly three-body abrasion) on in-bed tubes can occur by several causes. To date it is not clear to what extent materials wastage can be attributed to phenomena such as abrasion or erosion by the fluidized bed particles, and the predominance between erosion or abrasion as main forms of mechanical damage remains as an area of discussion. The aim of this work is to assess the effect of impact angle and mode of wear in terms of the observed morphologies of the exposed surfaces and 1) a dominant abrasion process derived from a simulated fluidized bed environment and Rabinowicz theory and 2) an erosion process, using Finnie´s erosion theory.

2. *Experimental Procedures*

2.1. Materials

Cylindrical specimens with typical dimensions of about 6 mm diameter and 24 mm length made from mild steel (in normalized condition) and 310 stainless steel (solution treated) were used. Table 1 shows the chemical composition (%wt) for the steels.

	C	S	P	Si	Mn	Cr	Ni	Mo	Fe
Mild steel	0.22	0.03	0.04	0.35	0.72	-	-	-	Bal.
310 SS	0.15	0.025	0.03	1.5	2.0	25	19	-	Bal.

Table 1. Chemical compositions (%wt) of the steels tested

Before exposure, the specimens were ground progressively to a final surface finish with 800 grit SiC paper using water as coolant, immediately rinsed in methanol, degreased with acetone and dried in a stream of hot air. The extent of damage to specimens exposed to the erosion rig was determined by weight change per unit area measurements using a Sartorious microbalance, with a resolution of 10^{-5} g.

2.2. Impact Angle Measurements

To assess the effect of impact angle on selected specimens after tests, thickness loss measurements were carried out using a profilometer system. Basically, the system consist of i) a specimen jig and its movement unit; ii) a stylus coupled with a LVDT transducer and iii) the acquisition unit. The specimen is positioned in the jig which is rotated horizontally about its axis by a stepper motor coupled to a gear box. To perform a measurement, a stylus is brought into contact with the specimen surface in a continuous mode, and any vertical displacement is taken up by movement of the core of a LVDT transducer with a linear displacement range of ± 1 mm and a reproducibility of 1 µm. Before the start of a run, the stylus was positioned on the area (trailing edge) that was not exposed to the particles in the bed environment, using this as a base line.

2.3. The Fluidized-Bed Rig

Experiments were carried out in a fluidized bed (FB) rig, which basically consist of a) a fluidized-bed chamber containing approximately 40 % vol. of particles during a test, b) a specimen holder system and c) a heating system. Fig 4 shows a schematic of the apparatus used. This consists of a light fluidized-bed of particles in which cylindrical specimens are rotated in the vertical plane into and out of the bed. For each temperature, a fluidizing velocity of 1.3 X Umf (where Umf is the minimum fluidization velocity) was used. Depending upon the angular velocity chosen, the linear velocity of the specimens relative to the particles is achieved.

2.3.1 Experimental Conditions

The experimental conditions used were the following: exposure temperatures from 100^{0}C up to 600^{0}C, and each test last 24 hours; air as oxidant gas*; the particles used were relatively angular alumina particles of 560 µm average size at impact velocities ranging from 1 m s^{-1} to 4.5 m $s.^{-1}$. Owing to degradation, the particles were replaced at regular intervals. Morphological examinations of wear scars were carried out using an AMRAY scanning electron microscope, linked with an EDX unit. The aim here was to assess the main trends of the effects of temperature and impact velocity and to characterize the extent of degradation of the specimens.*

3. Results and Analysis

3.1 Wastage as a Function of Temperature and Impact Velocity

3.1.1 Mild steel

Fig. 5 shows the behaviour of mild steel. At the lowest velocity and below 250^{0}C, no weight losses were recorded. Further increases in temperature resulted in small weight gains (negative scale). At 2 m s^{-1} and temperatures above 500^{0}C, this trend changed, and small weight losses were recorded. In the velocity range of 2.5 m s^{-1} to 4 m s^{-1}, a wastage peak was observed. This peak occurred at 300^{0}C, for impact velocities up to 3.5 m s^{-1}, but between 300^{0}C and 350^{0}C at 4 m s^{-1}. The weight losses had a minimum at 450^{0}C, and, above this temperature, significant increments in weight loss were recorded. At 4.5 m s^{-1}, no wastage peak was observed only a continuous increase in weight loss with temperature.

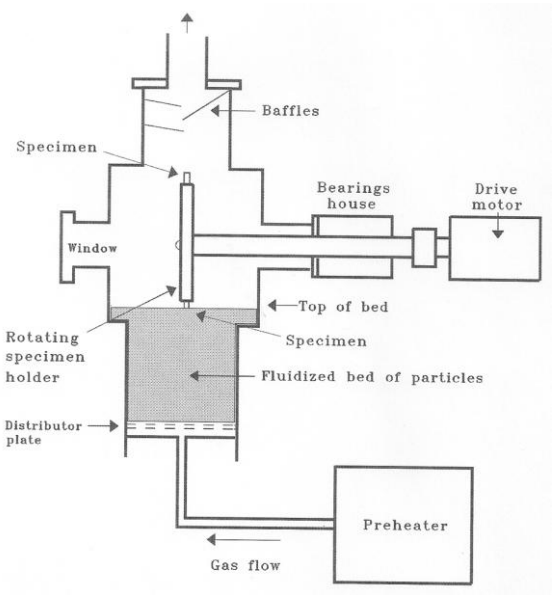

Fig. 4 Schematic diagram of the fluidized-bed apparatus used.

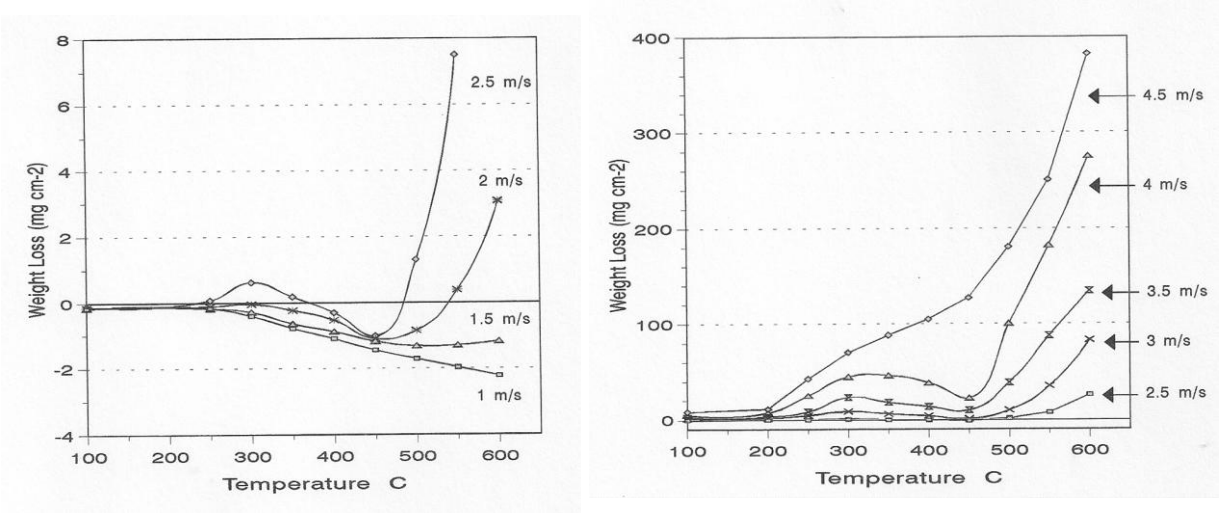

Fig. 5 Weight change as a function of temperature and specimen velocity for mild steel exposed in the FB rig with the 560 µm alumina particles for 24 h.

Fig. 6 shows the morphology after exposure at 250^{0}C and 1.5 m s^{-1}. Here, the surface consisted mainly of compacted erodent (and erodent debris). X-ray mapping on the surface gave evidence for this. At 300^{0}C and 2.5 m s^{-1}, a rather different morphology was observed: the surface had a polished appearance, and, at higher magnification, a thin (apparently less than 1 µm thick) scale was observed, Fig. 7. At 450^{0}C and 2.5 m s^{-1}, the surface had a rippled appearance, Fig. 8, whereas at 600^{0}C and 1.5 m s^{-1}, the surface was again rippled, and scale had apparently spalled from some areas, Fig. 9 (a). At 2.5 m s^{-1}, surface ripples were still noted, but, now, cracks in the surface scale were clearly seen, Fig. 9 (b). With further increase in velocity to 4.5 m s^{-1}, surface ripples were no longer observed but a dark polished surface was noted. At higher magnification, surface cracks were observed, Fig. 9 (c).

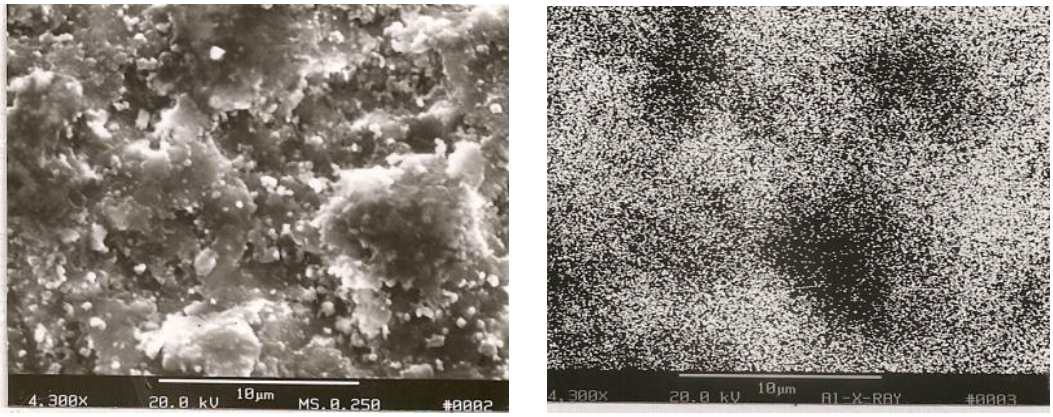

a) *b)*

Fig. 6 Scanning electron micrograph of mild steel exposed in the FB rig at 250^{0}C and 1.5 m s^{-1} showing a) the surface morphology and b) X-ray map of aluminum in a)

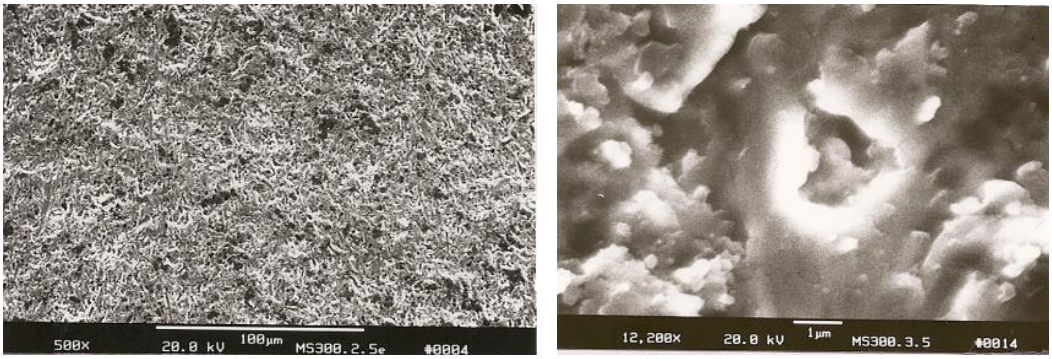

a) *b)*

Fig. 7 Scanning electron micrograph of mild steel exposed in the FB rig at 300^{0}C and 2.5 m s^{-1} showing a) the surface morphology and b) morphology at higher magnification

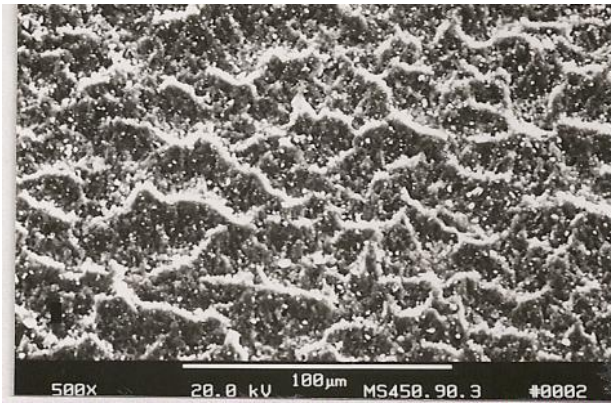

Fig. 8 Scanning electron micrograph of mild steel exposed in the FB rig at 450^{0}C and 2.5 m s^{-1}.

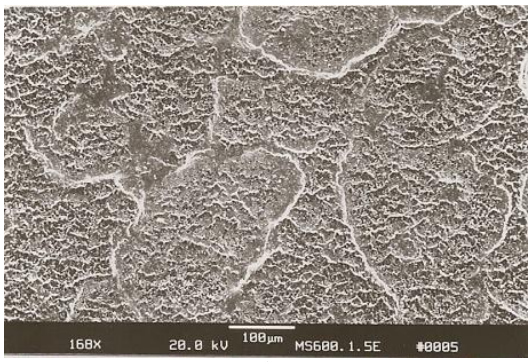

a)

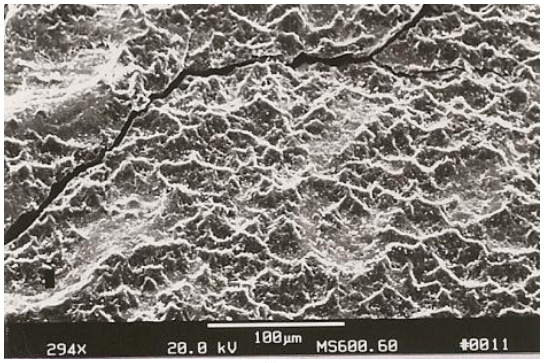

b)

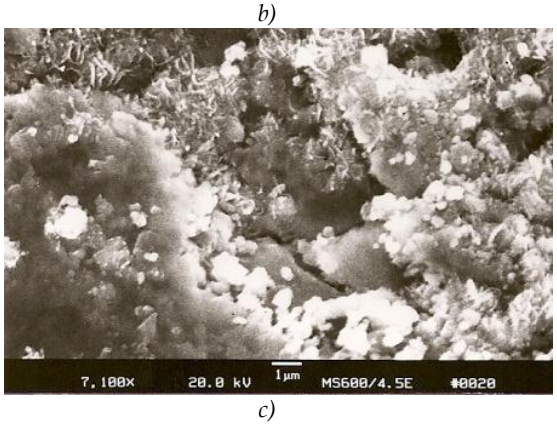

c)

Fig. 9 Scanning electron micrograph of mild steel exposed in the FB rig at 600^{0}C and at a) 1.5 m s^{-1}, b) 2.5 m s^{-1}, and c) 4.5 m s^{-1}

3.1.2 310 Stainless steel

A most distinctive feature of the weight loss of this steel as a function of temperature when compared with the mild steel is that, no weight loss peak was recorded, under any condition, Fig. 10. This is in contrast with previous laboratory studies from other groups in the early 1990s (Ninham et al., 1990, Stack et al., 1991, Stott et al., 1990) and this is attributed to the lower impact energies of these studies. The onset of weight loss over all the temperature range was found to be strongly dependent on impact velocity. For example, at 1 m s^{-1} no weight loss was recorded at temperatures below 500^{0}C. Increasing velocity reduced quite significantly this "threshold" temperature. At 2 m s^{-1} it fell to 300^{0}C, and at 4.5 m s^{-1} it was less than 100^{0}C. Above this "threshold" temperature, the weight loss increased non-linearly with temperature in all cases. At 100^{0}C, the behaviour was similar to that of the mild steel, i. e., below 2.5 m s^{-1} no weight loss was observed, and, above this velocity, the weight loss increased non-linearly. For this steel, the extent of weight loss increased with increasing temperature for a given impact velocity. It is interesting to note that, at the lower velocities (1-l.5 m s^{-1}) the weight changes were relatively independent of velocity for both steels. However, at the high velocities (i.e. >1.5 m s^{-1}) the increase in wastage rate for mild steel as a function of increasing velocity was much greater than for the 310 stainless steel. Weight gains were recorded at the lower velocities for both materials. Indeed, this was the case for 310 stainless steel even at 2.5 m s^{-1}. At 600°C, the increase in wastage rate as a function of velocity differed from that at the lower temperature, while the overall rates were much higher than at 300°C. In the lower velocity range (1-2 m s^{-1}) the erosion-corrosion rate of the 310 stainless steel was higher than that of the mild steel. However, the results also showed that the ranking order of degradation rates of the alloys changed

as a function of velocity. For example, at 2 m s^{-1} the weight loss of 310 stainless steel was approximately a factor of 10 greater than for the mild steel. At 2.4 m s^{-1}, however, there was no difference between the wastage rates of both materials, while above this velocity, the relative wastage rates of the alloys reversed, with the mild steel now giving a higher value than the 310 stainless steel.

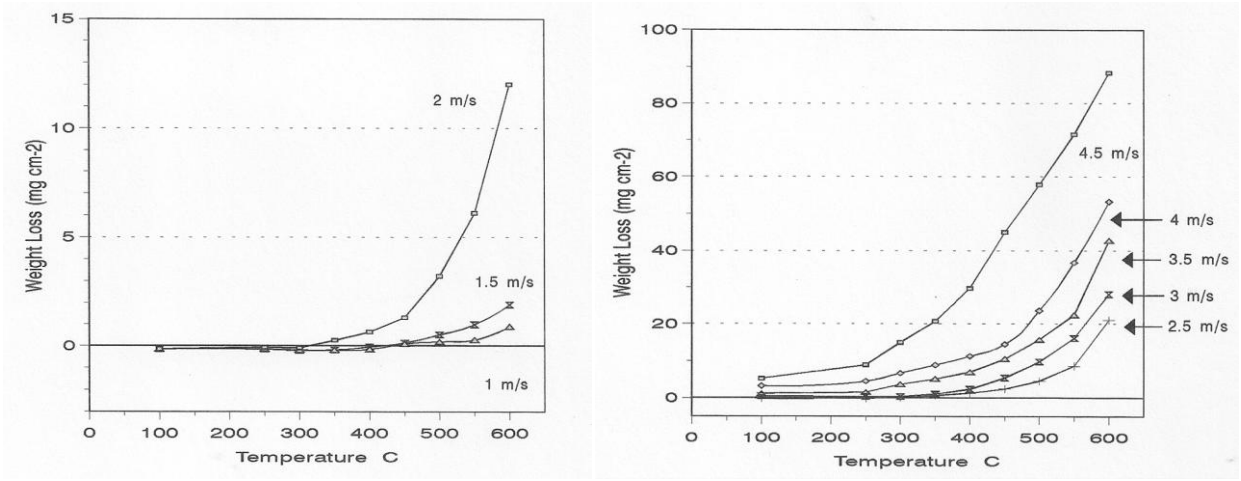

Fig. 10 Weight change as a function of temperature and specimen velocity for 310 SS exposed in the FB rig with the 560 µm alumina particles for 24 h.

In general, impact velocities up to and below 2.5 m s^{-1} produced rippled surfaces at all temperatures. Figures 11(a), 11(b) and 11(c) show examples of surface morphologies after exposure at 300^{0}C and 1.5 m s^{-1}, 450^{0}C and 2.5 m s^{-1}, and 600^{0}C and 1.5 m s^{-1}, respectively. However, such ripples were not observed at impact velocities above 2.5 m s^{-1}. As an example of this, Fig. 12 (a and b) shows the surface morphology after exposure at 600^{0}C and 4.5 m s^{-1}, where wear tracks of about 10 to 20 µm in length and areas of scale spallation could be observed.

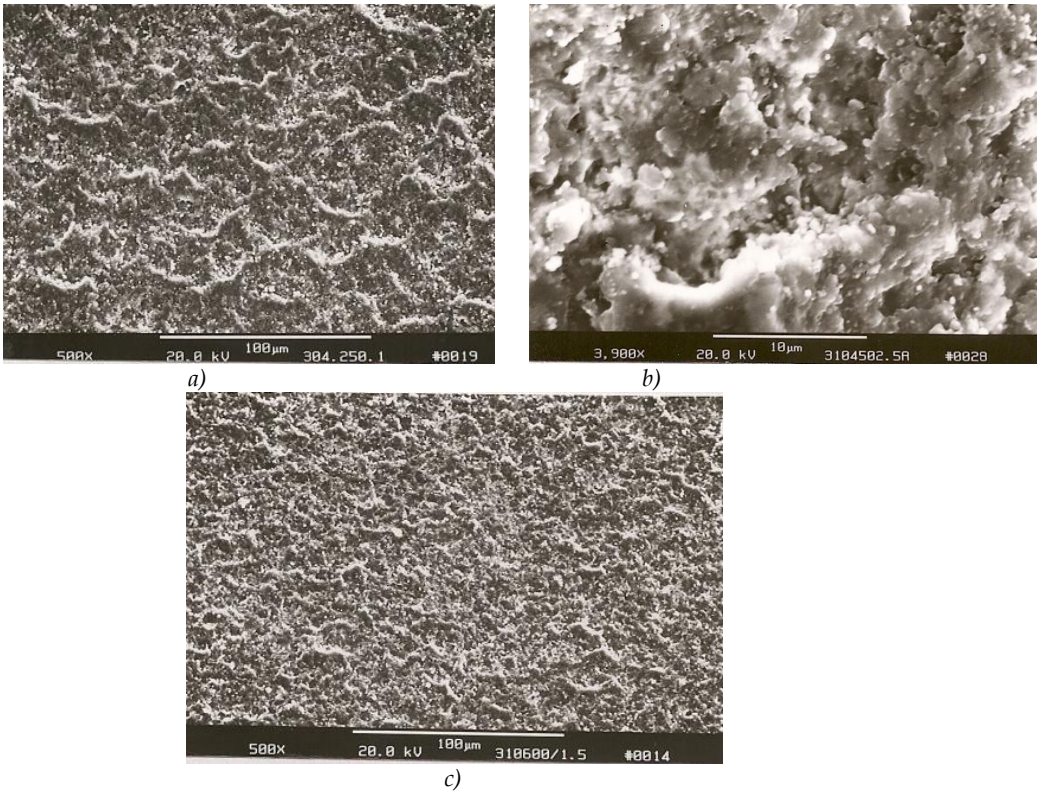

a) *b)* *c)*

Fig. 11 Scanning electron micrograph of 310 stainless steel exposed in the FB rig at a) 300^{0}C and 1.5 m s^{-1}, b) 450^{0}C and 2.5 m s^{-1}, and c) 600^{0}C and 1.5 m s^{-1},

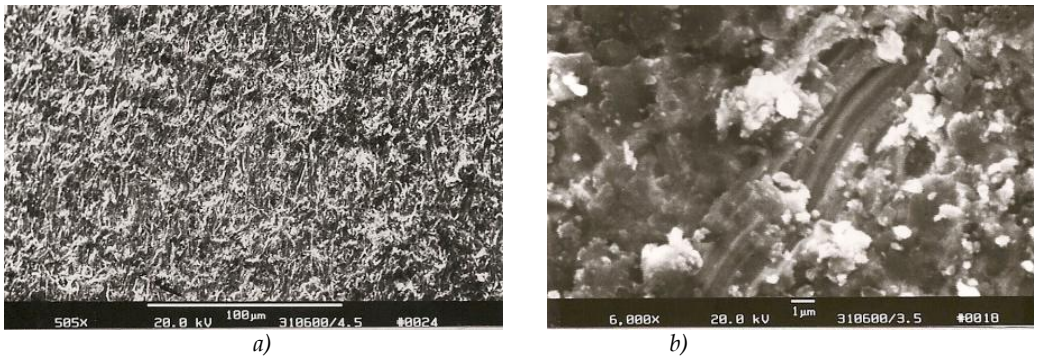

a) b)

Fig. 12 Scanning electron micrograph of 310 stainless steel exposed in the FB rig at a) 600^{0}C and 4.5 m s^{-1}, b) magnification of a)

3.2 Wear Pattern

Fig. 13 shows the angular dependence on thickness loss for mild steel and 310 SS at 100^{0}C. In the first case, two wear profiles are shown: at 1.5 m s^{-1}, a negative thickness was recorded in the angular range from 0^0 to 180^0. More likely, this pattern could be associated with deposition of erodent on the exposed area, as was confirmed by EDX analysis on the specimen surface. Indeed, this was the case for both steels at such low velocity and below 300^{0}C. Increasing the impact velocity produced a typical M pattern with two peaks located at each side from the front of the specimen. For instance, at 4.5 m s^{-1}, the maximum thickness loss was about 30 µm, although some material loss was also evident at normal impact angle. For the 310 SS, a similar trend was found, although the thickness loss was slightly less at both shallow and normal impact angles, compared with the mild steel. For both steels, the angle of maximum attack was almost the same, about 35^0 (145^0). The angle in the parenthesis corresponds to the second peak of the pattern.

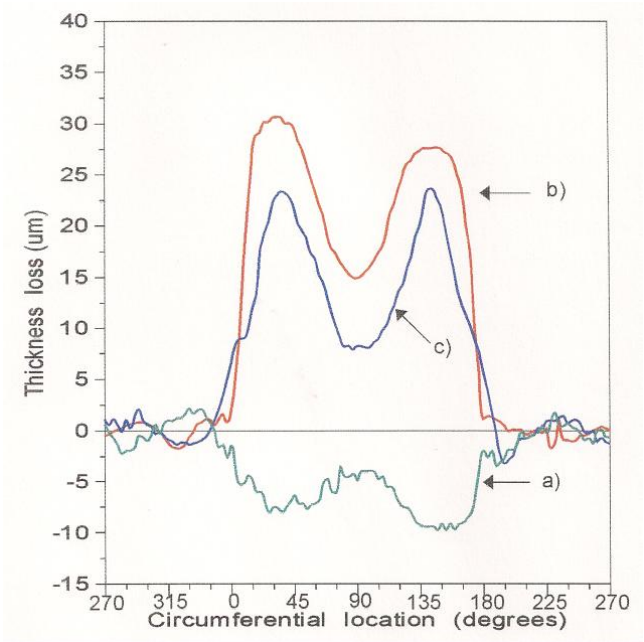

Fig. 13 Thickness loss as a function of impact angle for mild steel at 100^{0}C eroded with the 560 µm alumina particles at a) 1.5 m s^{-1}, b) 4.5 m s^{-1} and c) 310 SS at 4.5 m s^{-1}

For mild steel at 300^{0}C and 450^{0}C, and impact velocities from 2.5 m s^{-1} to 4.5 m s^{-1}, the wear patterns found are shown in Fig. 14. At 300^{0}C, it can be seen that the maximum angle of wear shifts slightly to lower angles i.e., from 33^0 to 27^0 (147^0 to 153^0) with increasing speed. This also caused a large increase in thickness loss. At the highest speed, a maximum loss of about 115 µm was recorded, whereas the specimen front has a typical loss of 15 µm (a loss was not observed at lower speeds). At 450^{0}C, and 2.5 m s^{-1}, no thickness loss was recorded, but further increases in impact velocity produced similar profiles to the ones observed at 300^{0}C. At the highest velocity, the wastage at the specimen front was somewhat higher, with a V shape pattern. At shallow angles, the main difference at both temperatures was the thickness loss magnitudes. Fig. 15 shows the results at 600^{0}C for mild steel. Here the angle of attack shifted from 33^0 to 24^0 (147^0 to 156^0) on increasing the impact velocity from 2.5 m s^{-1} to 4.5 m s^{-1}.

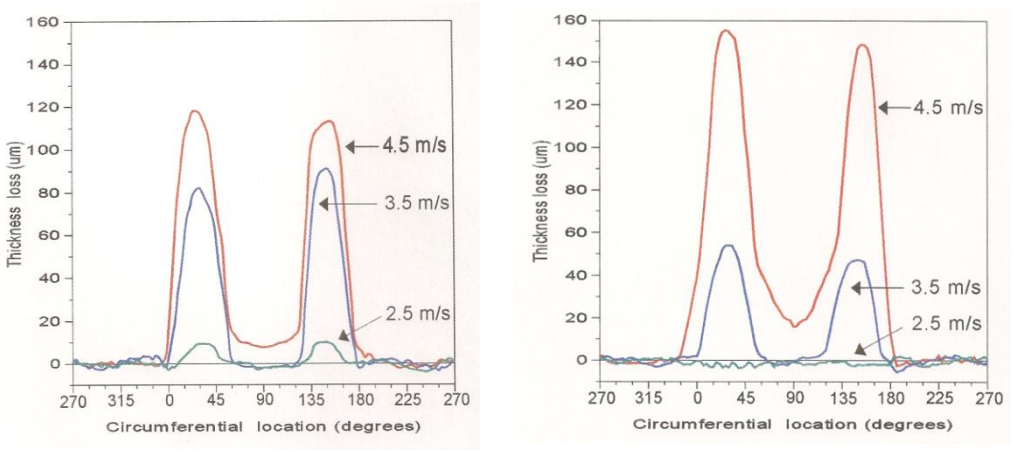

a) 300⁰C *b) 450⁰C,*

Fig. 14 Thickness loss as a function of impact angle for mild steel at a) 300⁰C and b) 450⁰C, eroded with the 560 µm alumina particles.

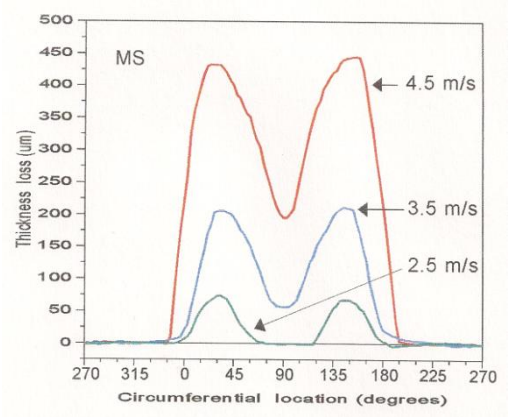

Fig. 15 Thickness loss as a function of impact angle for mild steel at 600⁰C eroded with the 560 µm alumina particles.

The wear profiles for the 310 SS as function of impact velocity at 300⁰C and 450⁰C are shown in Fig. 16. In general, on increasing velocity from 2.5 m s^{-1} to 4.5 m s^{-1}, the angle of attack changed from 33⁰ to 27⁰ (147⁰ to 153⁰) at 300⁰C, and from 30⁰ to 24⁰ (147⁰ to 156⁰) at 450⁰C. The patterns were quite similar, but it can be noted that, for each velocity, the wastage increases with increasing temperature. At 600⁰C the maximum angles of attack were about the same as the ones at 450⁰C, although there was a significant increase in the angular range of attack at both sides of the front, in particular at the highest speeds, Fig. 17.

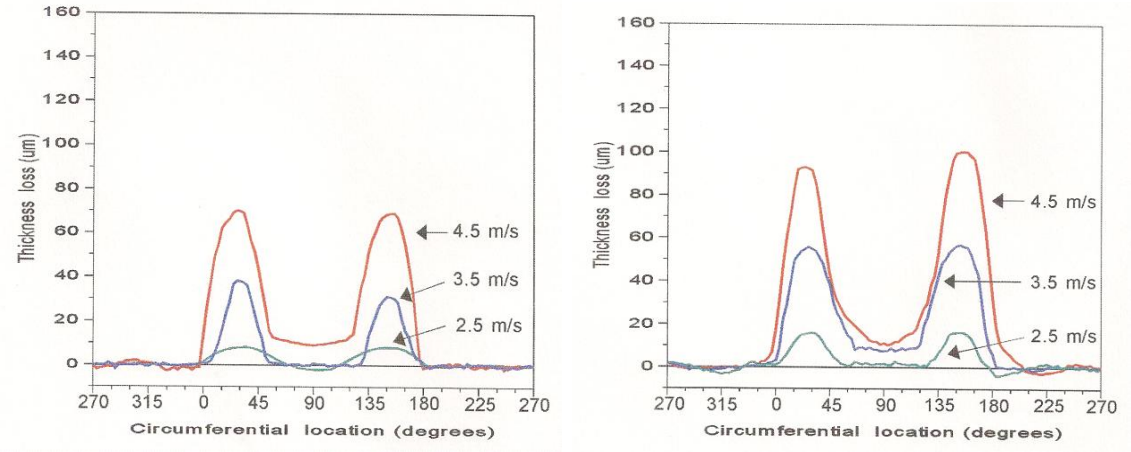

a) 300⁰C *b) 450⁰C,*

Fig. 16 Thickness loss as a function of impact angle for 310 SS at a) 300⁰C and b) 450⁰C, eroded with the 560 µm alumina particles.

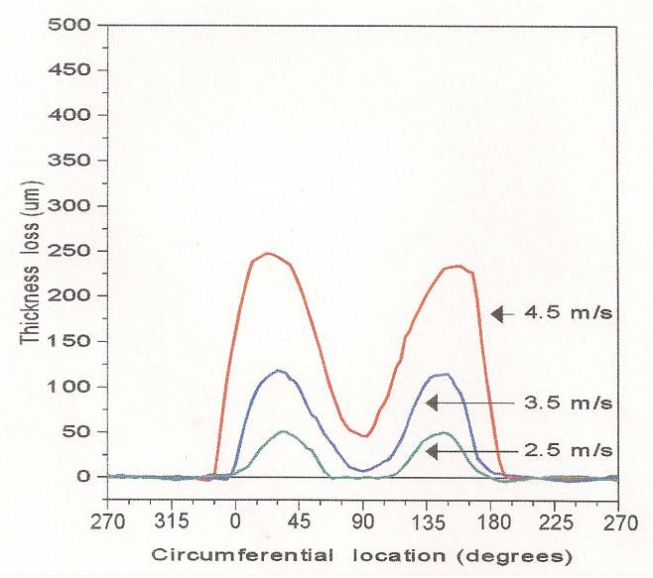

Fig. 17 Thickness loss as a function of impact angle for 310 SS at 600^{0}C eroded with the 560 µm alumina particles.

Regarding the location of maximum wastage observed in FBCs, this typically occurs at the tube bottom (90^0, Class B), or at about 60^0- 70^0 (Class A) on either side of the tube bottom, as depicted in Figure 3. In the present study, the angle of maximum wear was in the range from 20^0- 35^0. These values are small compared with the previous A classification, but this could be due to the possible differences in particle flow. On the other hand, the present results on the maximum angle of wear are in good agreement with the wear pattern reported on evaporator tubes in FBC units (Parkinson et al., 1985, Tsutsumi et al., 1989).

3.3 Effect of Impact Angle and Mode of Wear

Due to the nature of the bed, the environment in a fluidized bed may produce wear which can resemble either a three-body abrasion process or an erosion process. In the former, particles can be pressed against each other and slide over the tube surface, whereas, in the latter, particles act independently of each other, leaving the surface after impact. Although some valuable information on bed behavior has been reported in the last few years, there is still controversy about which process may dominate. On the basis of the results obtained in section 3.2, an attempt is made to describe the bed environment in terms of firstly, a dominant abrasion process, and, secondly, an erosion process. In the first case, according to Rabinowicz (Rabinowicz, 1965) the abrasive wear process is considered to be proportional to the contact pressure exerted by the particle flow multiplied by the local velocity on the specimen surface, whereas, in the second, Finnie's erosion theory has been considered (Finnie, 1960, Finnie, 1972).

3.3.1 Bed Environment in the FB Rig

Since the FB rig was operated at 1.3 x U_{mf}, gas velocities of about 0.17 m s^{-1} were achieved when using the larger particles. Under these conditions, Tsutsumi's equation (eq. 1), predicts particle velocities of about 0.89 m s^{-1}. Therefore, the velocity of particles in the bed is assumed to have no significant effect on the wear of specimens, which, in turn, is dependent only on the velocity of the specimens.

3.3.2 Abrasive Wear

The flow regime in the bed is described by the Reynolds number, Re. Here, a continuous medium is considered; therefore

$$\mathrm{Re} = \frac{2\rho_b * U_0 * a}{\mu_b} \qquad (3)$$

Where: ρ_b = bed density, in the present case ~ 2300 kg m^{-3}; U_0 = specimen velocity relative to the particles, m s^{-1} ; a = specimen radius = 0.003 m ; μ_b = bed viscosity ~ 1.2 kg m^{-1} s^{-1} (value for a bed with 500 µm average size silica particles, (Grace, 1970)

Considering the velocity extremes in this work, i.e. 1 m s^{-1} and 4.5 m s^{-1}, this gives Re = 11.5 and Re = 51.7, respectively. In order to estimate the contact pressure, it is assumed that the particle and gas flows are uniform and behave as continua Fig. 18 shows a schematic diagram of the system under consideration.

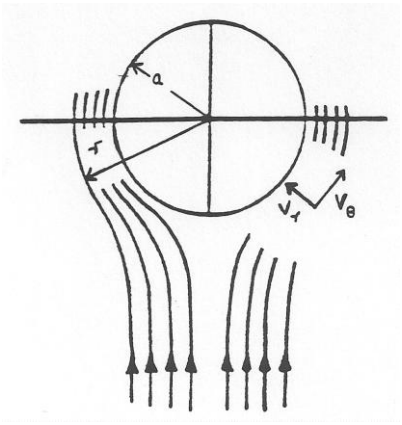

Fig. 18 Schematic diagram of flow pattern on specimens inside the bed of particles, indicating the components of velocity, Vr and V_θ.

Here, the potential fluid flow function, Φ, (in plane polar coordinates) is expressed by (Douglas et al., 1984, Kay & Nedderman, 1974)

$$\Phi = U_0\left(r + \frac{a^2}{r}\right)\cos\theta \tag{4}$$

Where r represents a point in a streamline, θ is the angle considered and a is the specimen radius. For flow around a cylinder, the radial ($V_{r\,(p,g)}$) and tangential ($V_{\theta\,(p,g)}$)components of velocity for the particles and fluidizing gas in terms of velocity potential are given by

$$V_{r(p,g)} = \frac{\partial\Phi}{\partial r} = U_0\left(1 - \frac{a^2}{r^2}\right)\cos\theta \tag{5}$$

$$V_{\theta(p.g)} = \frac{1}{r}\frac{\partial\Phi}{\partial\theta} = -U_0\left(1 + \frac{a^2}{r^2}\right)\sin\theta \tag{6}$$

At the surface of the cylinder, r = a , hence

$$V_{r(p,g)} = 0 \tag{7}$$

$$V_{\theta(p,g)} = -2U_0\sin\theta \tag{8}$$

Now, from Bernoulli´s equation, the pressure exerted by the particle (P_p) and gas (P_g) is given respectively by:

$$P_p = P_\infty + \frac{\rho_p}{2}\left(U_0^2 - V_\theta^2\right) \tag{9}$$

$$P_g = P_\infty + \frac{\rho_g}{2}\left(U_0^2 - V_\theta^2\right) \tag{10}$$

The difference between (6.8) and (6.9) gives the net pressure acting on the cylinder surface, thus

$$P_p - P_g = \frac{1}{2}\left(\rho_p - \rho_g\right)\left(U_0^2 - V_\theta^2\right) \tag{11}$$

$$P_p - P_g = \frac{U_0^2}{2}\left(\rho_p - \rho_g\right)\left(1-\left(\frac{V_\theta^2}{U_0^2}\right)\right) \tag{12}$$

Now, from eqn. (6.4), and assuming that, in general, the gas density is much lower than the particle density, the pressure distribution on the cylinder is given by

$$C_p = \frac{P_p - P_g}{\frac{1}{2}\rho_p U_0^2} = 1 - 4\sin^2\theta \tag{13}$$

Where Cp is the pressure coefficient. A plot of equation 13 is given in Fig. 19(a), where it can be seen that the pressure distribution is similar to that found at low Re numbers, Fig. 19(b). From classical abrasion theory (Archald, J. 1953, Rabinowicz, E. 1960), the abrasive wear rate, AWR, can be expressed as

$$AWR \propto V_\theta\left(P_p - P_a\right) \tag{14}$$

And, from eqns. (8) and (13)

$$AWR \propto U_0^3 \rho_p \sin\theta(1 - 4\sin^2\theta) \tag{15}$$

From this equation, Fig. 20 (curve A) shows the dependence of the predicted AWR on impact angle. The maximum wear is about 15° from the stagnation point, which is close to the specimen front. Hence, the above equation is not in agreement with the actual observations, where the maximum wear was observed in the range 24°to 33°. In a bubbling fluidized bed, a schematic diagram of the interaction between bubbles and a tube can be seen in Fig. 21. The region in the lower part of the bubble is the wake region, which carries entrained particles. Here, the measured wake angle is, $\theta_w \approx 120°$, as depicted in Fig. 21, for silica sand particles of 500 µm mean size (Rowe & Partridge, 1965). To some extent, when a bubble passing a tube, it appears that this angle may have some effect on the location of wear. Equation 15 thus may be modified by taking into account an angle given by $\theta_{wa} = \theta_w/2 \approx 60°$. Consider a case where the flow is modified by changing θ by θ - (θ_{wa} - 15°), where the 15° value is the difference of the angle at normal impact and the angle of maximum wear previously found. The result can be seen in fig. 20 (curve B), where the maximum angle of wear appears at about 60°, which corresponds with a 30° angle for the actual specimens, and correlates well with the experimental findings. However, it predicts higher wear at normal impact angle, which is not the case for the specimens in the present work. Now, suppose θ is changed by an amount equal to (θ - θ_{wa}) in equation 15. The result is given in Fig. 20 (curve C). Here, the maximum angle of wear at shallow angles is about 15°, this being lower than the observed range. Also, this last change predicts even a higher wear rate at the front of the specimen.

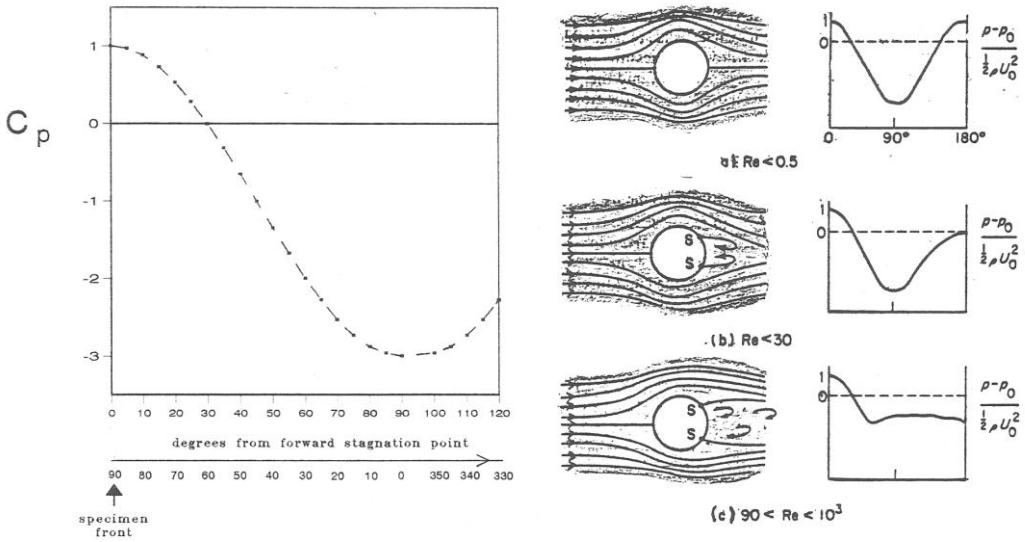

a) *b)*

Fig. 19 Coefficient of pressure, C_p, on the surface of a cylinder as a function of angle, a) as derived from equation 13, b) for flow past a cylinder for various Re ranges

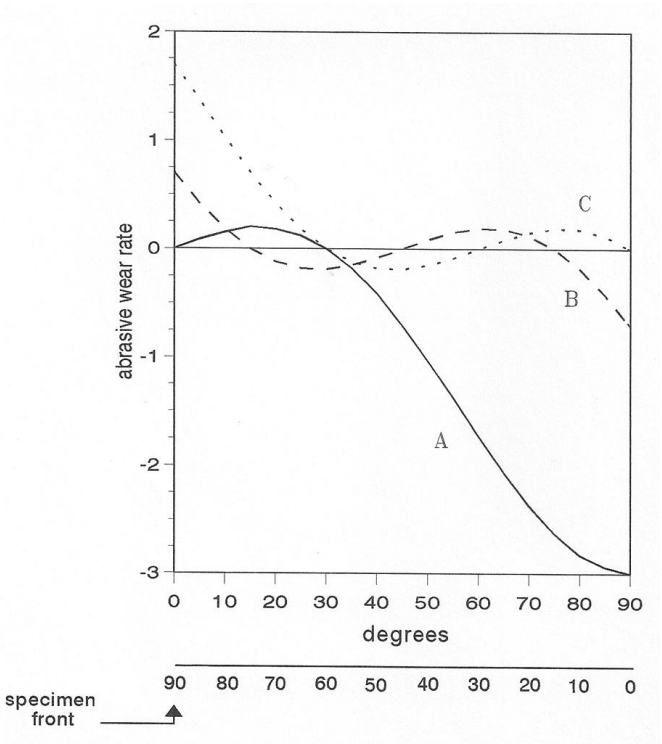

Fig. 20 Variation in abrasive wear rate as a function of impact angle, as predicted by abrasion theory: i) curve A resulting from equation 15; ii) curve B when changing θ by θ-(θ$_{wa}$-15°) in equation 15, and iii) curve C, changing θ by (θ-θ$_{wa}$) in equation 15.

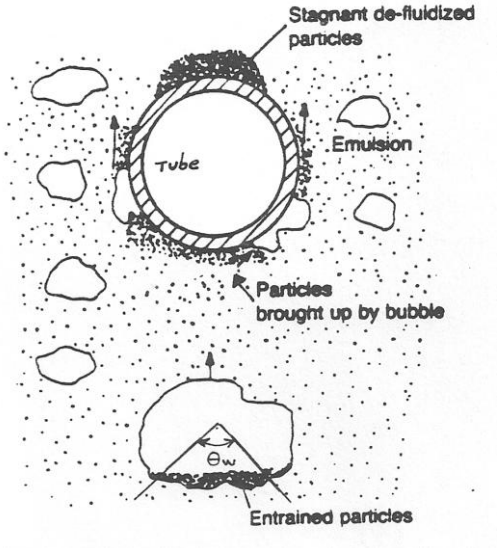

Fig. 21 Conditions near a tube immersed in a fluidized bed. θ$_w$ is the wake angle.

3.3.3 Erosive Wear

Finnie's classical erosion theory has been used in an attempt to correlate the present results on the effect of impact angle with the extent of erosion. The erosion rate expressed as volume loss, E$_v$, is related to the particle impact velocity, U, and angle of impingement, θ, by

$$E_v \propto U^n \cos^2 \theta \tag{16}$$

Where n is the velocity exponent (usually between 2 and 3). However, when the erosion rate is estimated by thickness loss, E$_t$, equation (16) may simply be multiplied by sin θ (Finnie, I. 1960). Since the results for the effect of impact angle were given as thickness loss, the resulting expression is

$$E_t \propto U^n \cos^2\theta \sin\theta \qquad (17)$$

This equation is plotted in Fig. 22. As would be expected, the predicted peak erosion angle, θ_{max} is ≈ 35°, which is in good agreement with the experimental results. However, it is worth noting that these results, Figs. 13 to 17, showed that, at low temperature, i.e. 100°C, and 4.5 m s^{-1}, θ_{max} was found at about 35°, whereas at 2.5 m s^{-1} and 300°C, θ_{max} was very similar to the previous value. This suggests that, at low temperatures, the impact velocity apparently had little effect on the peak erosion angle. At higher temperatures, θ_{max} shifted slightly to lower angles with increasing velocity from 2.5 m s^{-1} to 4.5 m s^{-1}. This is because changes in particle flow may take place as a function of both temperature and velocity. At the highest velocity used, increasing temperatures also shift θ_{max} to lower angles, (see for example Figs. 13 and 15). This suggests that the steels exhibit a more ductile behavior with temperature. Another observation is that, at least for the alloys studied, θ_{max} seems to be independent of the steel type.

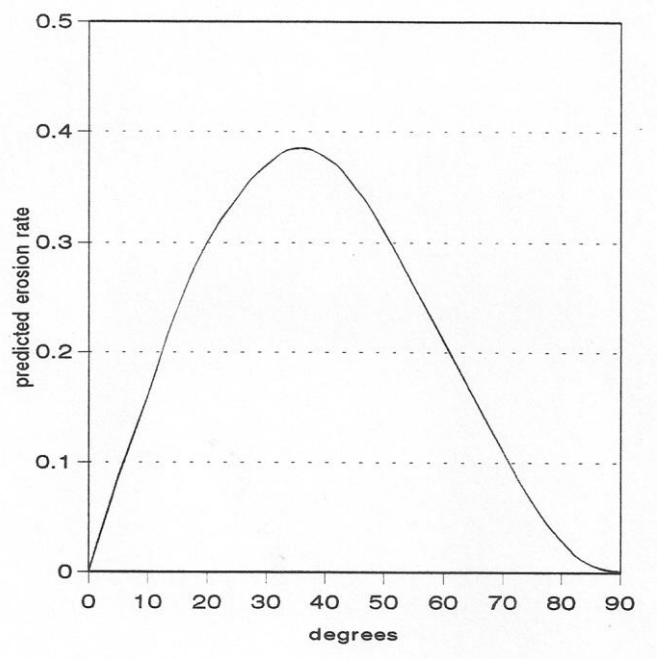

Fig. 22 Predicted erosion rate as a function of impact angle according with Finnie´s erosion theory. The angle of maximum attack is about 35^0. The specimen front is at the 90^0 angle.

In general, with the larger particles, ripple formation was a typical feature (which is generally associated with a purely erosion process) for most steels exposed at velocities up to about 3 m s^{-1}. Higher velocities produced surface morphologies that were dependent on the type of steel. For instance, for the low alloy steels, polished surfaces were not uncommon, whereas, for the stainless steels, a more clear ploughing and cutting action was observed. The wear tracks developed mainly on the 310 SS are consistent with a dominant abrasion process. However, very similar morphologies (showing cutting/ploughing action) for low alloy steels and stainless steels have been reported in tests carried out in more conventional rigs (Morrison et al., 1986, Zhou & Bahadur, 1990).

3.3.4 Comparison Between Abrasion and Erosion Theories

Based on the modifications made in the abrasion theory, leading to the behaviour given by curve B, Fig. 20, both theories predicted about the same peak angle wear, but only at low impact angle. The abrasion theory predicts higher wastage rates at normal impact angle, i. e. at the specimen front, while the erosion theory predicts no wastage at this location. This was normally the case at velocities typically bellow 4.5 m s^{-1}. Under mild fluidization conditions in a cold FB rig, it was found the formation of an air film directly below a cylindrical obstacle (Glass & Harrison, 1964). At this location (stagnant point) the gas and particle flows are at minimum values. Another possibility is the preferential embedment and deposition of very fine erodent particles that occur at normal impact angle compared with low angles. This may have modified the wastage rate here due to a shield effect. However, in general, exposure at temperatures above 300^{0}C and velocities above 2.5 m s^{-1} produced some wastage at the front of the specimens, clearly minimizing the previous effects. Taking the angular distribution of wear as a reference, it is very difficult to determine which form of wear may dominate, since a FB environment includes a dilute phase erosive condition and also a dense (continuous) phase abrasive condition. Disagreement between researchers is not uncommon; for instance, in one study, it was suggested that abrasion is responsible for the wear at the bottom of tubes (Stringer & Wright, 1987); however, at the same location another report concluded that wastage is by erosion only (Wheeldon, 1990). On the basis of purely morphological features, the present results suggest that the main form of wear

is one of an erosive nature. This agrees well with the results obtained in a FB rig facility, where erosion was the main form of wastage, but with a small amount of three-body abrasion contributing to the damage (Wang et al., 1993)

4. Conclusions

1. *A temperature of peak wastage (PWT) was observed for mild steel at about 300^{0}C but only within a certain velocity range i e., 2.5 m s^{-1} < PWT ≤ 4 m s^{-1}. The wastage of the 310 SS as a function of temperature did not show any peak wastage for the velocities studied in this work.*

2. *In general, erodent deposition was a dominant process at impact velocities below 3 m s^{-1} and temperatures below about 300^{0}C, regardless of the type of steel. The impact angle at which wear was a maximum was about 20^0-30^0 on each side of the leading point. Regarding this observation, it is worth noting that the results showed that at the lower temperature and the highest velocity used, the peak wastage angle, θ_{max}, was found at about 35^0, whereas at 300^{0}C and 2.5 ms^{-1} was very similar. At low temperatures, the impact velocity apparently had little effect on the peak wastage angle. At higher temperatures, θ_{max} shifted slightly to lower angles with increasing velocity from 2.5 ms^{-1} to 4.5 ms^{-1}. At the highest impact velocity used, increasing temperatures also shift θ_{max} to lower values. This suggests that the steels exhibit a more ductile behavior with temperature.*

3. *A further observation is that, at least for the steels used here, θ_{max} seems to be independent of the steel type.*

4. *On the basis of wear patterns found as a function of impact angle, an attempt has been made to define the probable modes of wear i.e. abrasion vs. erosion. The modified abrasion theory predicts well the wear pattern at shallow angles, but predicts higher wastage rates at normal impact angle, i.e. at the specimen front. On the other hand, erosion theory predicts maximum wear at an impact angle of 35^0 and no wear at the specimen front. Thus both theories have drawbacks with respect to damage in the FB rig.*

5. *Under the conditions of temperature and velocity considered, the wear losses were greater at shallow impact angle compared with the specimen front diminishing the importance of abrasion.*

6. *Following exposure to the test conditions, the formation of ripples, which are a feature of a purely erosive process, were often observed. Wear tracks were also observed, in particular at the highest velocities. These last features could be related to abrasive wear.*

4. Acknowledgments

The authors are grateful to CONACyT (Mexico) for supporting this work. Also we would like to express our thanks to Dr. Jiang Jiaren for permission to use his profilometer system, and to Gabriela K. Pedraza-Basulto, MSc., Adan Borunda-Terrazas, MSc., and Gregorio Vazquez-Olvera, MSc., for technical support.

5. References

Anderson, J., Carls, E. Mainhardt, P., Swift, W. Wheeldon, J., Brooks, S. Minchener, A. & Stringer J. (1987).Wastage of In-Bed Heat Transfer Surfaces in the Pressurized Fluidized Bed Combustor at Grimethorpe. *J. Eng. Gas Turbines and Power,* Vol.109, No.3, (July 1987), pp. 298-303, ISSN 0022-0825

Archald, J. (1953). Contact and Rubbing of Flat Surfaces. *J. Appl, Physics,* Vol.24, No.8, (Aug. 1953), pp. 981-988, ISSN 0021-8979

Beacham, B. & Marshall, A. (1979). Experiences and Results of Fluidized Bed Combustion Plant at Renfrew. *J. Inst. Energy,* Vol.52, No.411, (July 1979), pp. 59-64, ISSN 0144-2600

Boiarski, A. (1978) Testing, Identification and Evaluation of Advanced Experimental Materials and Coatings in the Design Conditions for Simulated Fossil Fuel Power Cycle Conditions, Task 2, *Batelle Report NTIS No. FE-2325-19, DOE Contract E(49-18)-2325, Dec 1978*

Douglas, J., Gasiorek, J. & Swaffield, J. (1984). Fluid Mechanics, 2nd Edition, Pitman Inst. Texts, London, ISBN-10 0273021346

Finnie, I. (1960). Erosion of Surfaces by Solid Particles. *Wear,* Vol.3, No.2, (March 1960), pp. 87-103, ISSN 0043-1648

Finnie, I. (1972). Some Observations on the Erosion of Ductile Metals. *Wear,* Vol.19, No.1, (Jan 1972), pp. 81-90, ISSN 0043-1648

Glass, D. & Harrison, D. (1964). Flow Patterns Near a Solid Obstacle in a Fluidized Bed. *Chem. Eng. Sci.,* Vol.19, No.12, (Dec. 1964), pp. 1001-1002, ISSN 0009-2509

Grace, J. (1970). The Viscosity of Fluidized Beds. Can. J. Chem. Eng., Vol.48, No.1, (Jan 1986), pp. 30-33, ISSN 1939-019X

Highley, J. & Kaye, W. (1983). Fluidized Beds Industrial Boilers and Furnaces, *Fluidized Beds: Combustion and Applications*, J.R. Howard (Ed.) 77-169, ISBN-0-8247-4699-6

Hou, P., MacAdam, S., Niu, Y. & Stringer, J. (2004). High Temperature Degradation by Erosion-Corrosion in Bubbling Fluidized Bed Combustors. *Materials Research,* Vol.7, No.1, (March 2004), pp. 71-80, ISSN 1516-1439

Howard, J.R., (I989) *Fluidization Technology*, Adam, Hulger, Bristol and New York. ISBN 0-85274-055-7

Janson, S. (1985). *Tube Wastage Mechanisms in Fluidized Bed Combustion Systems. Proceedings 8th Int. Conf. On Fluidized Bed Combustion*, pp. 750-759, ISSN: 0197453X, Springfield, Va, USA, March 18-21, 1985

Kantesaria, J. & P. Jukkola, D. (1983) Observations on Erosion of In-Bed Tubes in the Great Lakes AFBC. *Materials and Componenst Newlwtter US DoE,* No.46, (July 1987), pp. 6

Kay, J. & Nedderman, R. (1984). Fluid Mechanics and Heat Transfer, 3rd Ed. Cambridge University Press, ISBN-0521303036

Levy, A. (1987). , The Erosion-Corrosion of FBC, In–Bed Tubing Alloys, *EPRI Worshop on Wastage on In-Bed Surfaces in Fluidized Bed Combustors, Vol III* , pp. 1-73, Argonne, Illinois, USA, Nov 2-6, 1987

Mezko, J. (1977). *Metal Progress,* Vol. 112, pp.30

Montrone, E. (1987). Experience with Foster Wheeler FBC´S, *EPRI Worshop on Wastage on In-Bed Surfaces in Fluidized Bed Combustors, Vol III* , pp. 1-11, Argonne, Illinois, USA, Nov 2-6, 1987

Morrison, C., Scattergood, R. & Routbout, J. (1986). Erosion of 304 Stainless Steel. *Wear,* Vol.111, No.1, (Jan 1986), pp. 1-13, ISSN 0043-1648

Ninham, A. J., Hutchings, I. M. & Little, J. A. (1990). Erosion-Oxidation of Austenitic and Ferritic Alloys. *Corrosion,* Vol.46, No.4, (Apr 1990), pp. 296-301, ISSN 0010-9312

Oka, S. (2004). Fuidized Bed Combustion, Marcel Dekker, New York. ISBN 0-8247-4699-6

Parkinson, M., Napier, B., Jury, A. & Kempton, T. (1985). Cold Models Studies on PFBC Erosion, *Proceedings of 8th International Conference on Fluidized Bed Combustion Vol II*, pp. 730-738, ISSN: 0197453X, Springfield, Va, USA, Mach 18-21, 1985

Peeler, J. & Whitehead, A. (1982). Solids motion at horizontal tube surfaces in a large gas-solid fluidized bed *Chem. Eng. Sci.,* Vol.37, No.1, (Jan 1982), pp.77-82, ISSN 0009-2509

Rabinowicz, E. (1995). Friction and Wear of Materials, John Wiley & Sons, ISBN 0471830844

Rademarkers, P. & Kettunen, P. (1996). Materials Requirements and Selection for Fluidized Bed Combustors , *High Temperature Alloys for Gas Turbines and Other Applications 1986, Part 2*, W. Muntz (Ed.) 269-292, ISBN-13 978-9027723482

Rademarkers, P., Lloyd, D. & Regis, V. (1990). ABFC´S: Bubbling, Circulating and Shallow Beds In: *High Temperature Materials in Power Energy, Part 1,* E. Bachelet, (Ed.), 43-63, ISBN 978-0792309277

Rowe, P., & Partridge, B. (1965). An X-Ray Study of Bubbles in Fluidised Beds. *Trans. Inst. Chem. Eng.,* Vol.43, pp. 157-175, ISSN 0043-1648

Stack, M. M., Stott, F. H. & Wood, G. C. (1991). Erosion-Corrosion of Preoxidized Incoloy 800H in Fluidized Bed Environments: Effects of Temperature, Velocity and Exposure Time. *Mat. Sci and Tech,* Vol.7, pp. 1128-1137, ISSN 0267-0836

Stott, F. H., Stack, M. M. & Wood, G. C. (1990). The Role of Oxides in the Erosion-Corrosion of Alloys Under Low Velocity Conditions, *Proceedings*: *Corrosion-Erosion-Wear of Materials at Elevated Temperatures*, pp. 12-1 to -12-16, ISBN 1-877914-18-5, Berkeley, Calif, USA, Jan 31-Feb 02, 1990

Stringer, J. & Wright, I. (1987). Erosion/Corrosion in FBC Boilers, *EPRI Worshop on Wastage on In-Bed Surfaces in Fluidized Bed Combustors, Vol I* , pp. 1-30, Argonne, Illinois, USA, Nov 2-6, 1987

Tsutsumi, K., Tatebayashi, J., Hasegawa, K., Takamori, M., Okada, Y. & Furobayashi, K. (1989). Development of Erosion Resistant In-Bed Tubes. *Proceedings Int. Conf. On Fluidization (Fluidization VI)*, ISBN 0816904596, Banf, Alberta, Can. May 1989

Wang, B., Geng, G. & Levy, A, (1993). Effect of Microstructure on Materials Wastage in a Room-Temperature Fluidized-Bed Wear-Test Rig . *Wear,* Vol.165, No.1, (May 1993), pp. 25-33, ISSN 0043-1648

Wang, B. & Levy, A, (1992). Erosion-Corrosion of 1018 Steel at Eroded Low Velocities by Bed Material. *Wear,* Vol.155, No.1, (May 1992), pp. 137-147, ISSN 0043-1648

Wheeldon, J. (1990). A Re-Evaluation of Tube Wastage Data Collected from a Bubbling Fluidised Bed Cold Model *Proceedings*: *Corrosion-Erosion-Wear of Materials at Elevated Temperatures*, pp. 41-1 to 41-13, ISBN 1-877914-18-5, Berkeley, Calif, USA, Jan 31-Feb 02, 1990

Zhang, X. (1980). *Proceedings 6th Int. Conf. on Fluidized Bed Combustion***, OCLC**: 6896711, Atlanta, Ga, USA, April 9-11, 1980

Zhou, J. & Bahadur, S. (1990). Futher Investigations on the Elevated Temperature Erosion-Corrosion of Stainless Steels, *Proceedings: Corrosion-Erosion-Wear of Materials at Elevated Temperatures 1990*, A. Levy (Ed.) pp 13-1 to 13-17, ISBN 1-877914-18-5, Berkeley, Calif, USA, Jan 31-Feb 02, 1990